

Spatial heterodyne interferometry with polarization gratings

Michael W. Kudenov,^{1,*} Matthew N. Miskiewicz,¹ Michael J. Escuti,¹ and Eustace L. Dereniak²

¹Department of Electrical & Computer Engineering, North Carolina State University, 2410 Campus Shore Dr., Raleigh, North Carolina 27606, USA

²College of Optical Science, The University of Arizona, 1630 E. University Boulevard, Tucson, Arizona 85721, USA

*Corresponding author: mike.kudenov@ncsu.edu

Received August 17, 2012; revised September 20, 2012; accepted September 20, 2012;
posted September 21, 2012 (Doc. ID 174528); published October 19, 2012

The implementation of a polarization-based spatial heterodyne interferometer (SHI) is described. While a conventional SHI uses a Michelson interferometer and diffraction gratings, our SHI exploits mechanically robust Wollaston prisms and polarization gratings. A theoretical model for the polarization SHI is provided and validated with data from our proof of concept experiments. This device is expected to provide a compact monolithic sensor for subangstrom resolution spectroscopy in remote sensing, biomedical imaging, and machine vision applications. © 2012 Optical Society of America

OCIS codes: 120.3180, 300.6300, 300.6310.

Subangstrom (<0.1 nm) spectral resolution is required for many applications. Some include monitoring atomic emission lines for atmospheric wind speed and temperature [1], testing laser emission and stability [2], and astronomical studies of absorption within the interstellar medium [3]. Since the spectral resolution of grating-based spectrometers is restricted by the diffraction limit [4,5], interference methods are often used to achieve subangstrom resolution. Some favored instruments include the Fabry–Perot etalon (FPE) [6], Lyot filter [7], and spatial heterodyne interferometer (SHI) [8]. To confine this manuscript’s scope, we will only focus on the FPE’s and SHI’s limitations.

In an FPE, the cavity’s optical depth is scanned in time by changing its thickness, pressure, or spatial offset [9]. Measuring the transmitted intensity versus optical depth yields a high-resolution spectrum. Alternatively, an SHI can be used to avoid temporal scanning and reduce measurement time [10]. A conventional Michelson interferometer-based SHI is depicted in Fig. 1. Two diffraction gratings, G_1 and G_2 , are tilted by an angle ε such that one wavelength, λ_R , retrodiffracts back to the beamsplitter (BS). Meanwhile, other wavelengths diffract off-axis. This creates a spatially dependent optical path difference (OPD) that is heterodyned around λ_R . While this eliminates temporal scanning, it is challenging to make the interferometer monolithic and compact enough to mount directly onto an imaging array [11].

To avoid alignment, size, and stability issues associated with a Michelson interferometer, we describe a new polarization spatial heterodyne interferometer (PSHI). An operational concept of the PSHI is depicted in Fig. 2. A ray of polychromatic light is incident on a linear polarizer (P), which is oriented at 45° from the y axis. This is followed by a birefringent Wollaston prism (WP), with wedge angle α and linear polarization eigenmodes that are parallel to the x and y axes. An achromatic quarter waveplate (QWP) converts these linear eigenmodes into orthogonal circular polarization states, which then interact with a polarization grating (PG) [12–14]. Since the PG’s eigenmodes are circular, right and left circularly polarized light corresponds to $+1$ st and -1 st order

diffraction, respectively. Lastly, a linear analyzer (A) unifies the polarization state to produce interference.

Using the small angle approximation for the Wollaston prism’s wedge angle, α , and the PG’s diffraction angle, $\theta_{\pm 1}$, enables the angle exiting the PG to be calculated as

$$\theta_{\pm 1} = \Delta n \tan(\alpha) \pm \lambda/\Lambda. \quad (1)$$

where Λ is the PG’s period, $\Delta n = (n_e - n_o)$ is the birefringence, n_e and n_o are the extraordinary and ordinary refractive indices, respectively, and λ is the free-space wavelength. Transmission of the two beams through the analyzer unifies the polarization state, thereby enabling the two polarized beams to generate interference. Given spatially coherent illumination, the OPD is calculated by using the sag between the tilted planar wavefronts. This yields

$$\text{OPD} = 2x[\Delta n \tan(\alpha) - \lambda/\Lambda]. \quad (2)$$

Therefore, the OPD contains both achromatic and dispersive terms, which are contributed by the Wollaston prism and PG, respectively. Using the OPD, the two-beam interference pattern can be calculated as

$$I(x, y) = 1 + \cos(2\pi \text{OPD}/\lambda), \quad (3)$$

where λ appears in the denominator. Substituting the OPD into Eq. (3) produces

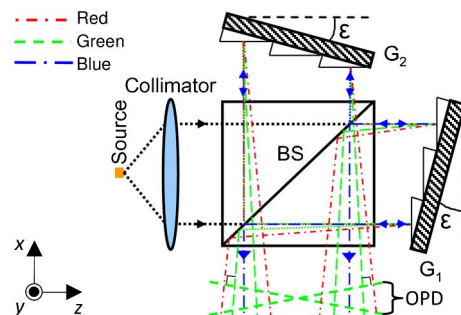


Fig. 1. (Color online) Michelson-based SHI. Wavefronts exit the BS tilted. Only green is shown for clarity.

$$I(x, y) = 1 + \cos(2\pi x[2\Delta n \tan(\alpha)\sigma - 2/\Lambda]), \quad (4)$$

where σ is the wavenumber ($\sigma = \lambda^{-1}$). From Eq. (4), we observe that the Wollaston prism generates the interference pattern common to birefringent Fourier transform spectrometers [15] while the PG provides a heterodyne offset. Therefore we have realized, to the best of our knowledge, the first common-path SHI that uses birefringent optics.

Another quantity, which was mentioned previously for the Michelson interferometer-based SHI, is the retrodiffraction wavelength λ_R . This is defined as the wavelength of light that corresponds to a spatial frequency of 0 cm^{-1} . Alternatively, it corresponds to the wavelength at which wavefront propagation, from the interferometer, is parallel to the optical axis (e.g., blue light in Fig. 1 and red light in Fig. 2). Since a PG is transmissive and not reflective, it does not have a retrodiffraction configuration. Therefore, the equivalent retrodiffraction wavelength, what we generally refer to as the heterodyne wavelength (λ_h), can be solved for by setting Eq. (2) equal to zero. This yields

$$\lambda_h = \Lambda \Delta n \tan(\alpha). \quad (5)$$

Proof of concept experiments have been conducted that demonstrate the PG's spatial heterodyning capability and the validity of Eq. (5). A layout of our experimental configuration is portrayed in Fig. 3(a). It consists of an illumination source (S) that can be either a tungsten halogen lamp or a monochromator. The source illuminates a diffuser (D) to provide spatially incoherent illumination to the quartz Wollaston prism (for quartz, $\Delta n = 0.0094$ at $\lambda = 440 \text{ nm}$). Our Wollaston prism has a $14 \times 14 \text{ mm}^2$ clear aperture, a 6.2° apex angle, and an added terminus thickness (t) of 0.85 mm . This terminus offsets the x position of zero OPD from $x_o = 0$ to $x_o = 3.92 \text{ mm}$ to enable collection of single-sided interferograms [16]. The prism is then followed by a QWP at 45° , and the prism's fringes are relocated on to the PG using an afocal relay (AR) with a measured magnification ratio (MR) of 1:0.965. Following the PG with an analyzing polarizer (A) and a second afocal relay (MR = 1:0.449) localizes the heterodyned fringes onto the focal plane array (FPA). It should be mentioned that the MR was measured by imaging the straightedges of a caliper in the plane of

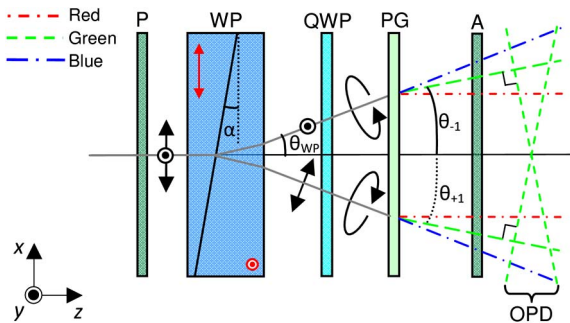


Fig. 2. (Color online) Diagram of the PSHI. Orthogonally polarized wavefronts exit the PG tilted. Note that only the green wavefronts (dashed lines) are shown for clarity and that a variation of these parts can be laminated together to form a monolithic part.

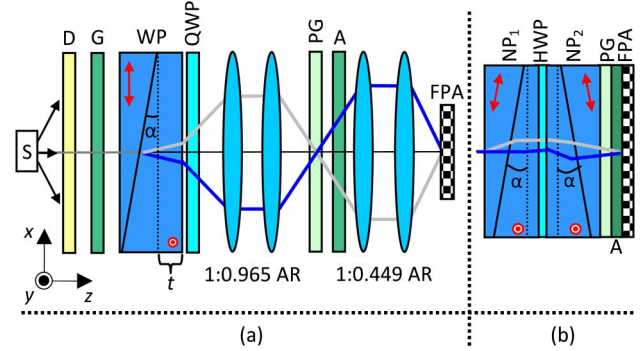


Fig. 3. (Color online) (a) Experimental proof of concept's layout for the polarization SHI. (b) Afocal relays can be removed to form a monolithic and compact device.

the PG and WP. Lastly, as demonstrated in our previous work [17], miniaturization can be realized with the system in Fig. 3(b). Here, fringes are relocated by two Nomarski prisms (NP_1 and NP_2) separated by a half waveplate (HWP). However, our experimental results were obtained using the setup of Fig. 3(a).

A PG, with a period of $\Lambda = 453 \mu\text{m}$, was used to spatially heterodyne the prism's interference. The PG was created by exposing a linear photoalignment material with a 325 nm laser. The exposure setup was similar to the one used in [18]. After exposure, the patterned structure was coated with a commercial liquid crystal polymer to achieve broadband half-wave retardation [12]. Accounting for the magnification factor between the prism and the PG makes the magnified heterodyne wavelength

$$\lambda'_h = \Lambda \Delta n \kappa \tan(\alpha), \quad (6)$$

where $\kappa = 0.965$ is the first relay's magnification. Therefore, the theoretical $\lambda'_h = 445.5 \text{ nm}$.

Verification of the heterodyne wavelength was accomplished by illuminating the diffuser with a monochromator. Illumination wavelengths spanned 450 to 710 nm in 2 nm increments. For each wavelength, the spatial interferogram was measured by the FPA and saved on a computer. MATLAB was then used to perform a least squares fit of

$$I = A + Q \cos(2\pi\xi(x - x_o)) \quad (7)$$

to the interferogram, where A is the offset, Q is the modulation's magnitude, ξ is the spatial frequency, and x_o is the interferogram's zero offset. The spatial frequency versus wavenumber is shown in Fig. 4, which enabled the calculation of a second order polynomial. Extrapolating this polynomial to $\xi = 0 \text{ mm}^{-1}$ yielded $\lambda_h = 445.8 \text{ nm}$: about 0.07% error with the theoretical value.

Next, white light illuminated the diffuser. Spatial interferograms were recorded for (a) the prism without the PG, (b) the prism with the PG and QWP at 45° , and (c) the prism with the PG and QWP at -45° . One-dimensional interferograms were calculated by averaging the two-dimensional interferograms along the y axis. Each case's interferogram is portrayed in Fig. 5(a)–5(c). Note that Fig. 5(b) and 5(c) show down- and up-shifted spatial

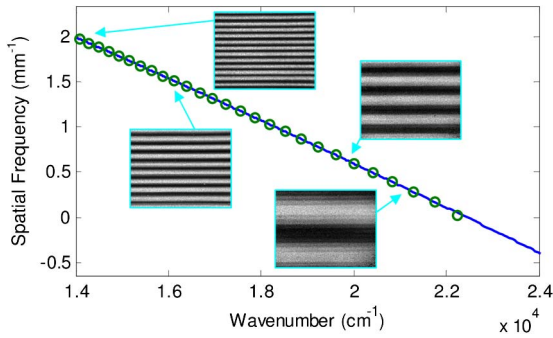


Fig. 4. (Color online) Measured spatial frequency versus wavenumber (circles) and a second order polynomial fit (solid line). Included are 2D images of the measured fringes at four wavenumbers.

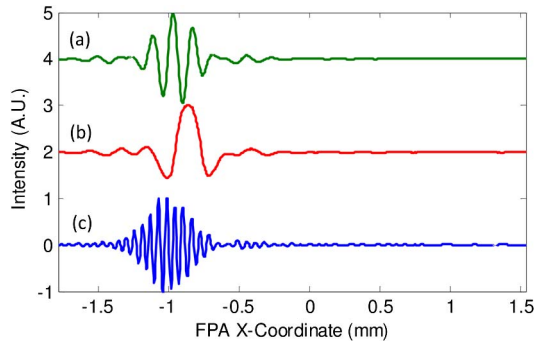


Fig. 5. (Color online) White light heterodyned interferograms. (a) Prism with no PG. (b) Prism and PG (45° QWP). (c) Prism and PG (-45° QWP).

frequencies, respectively. In the down-shifted case, a QWP orientation of $+45^\circ$ reduces $\theta_{\pm 1}$ of the PG's exiting wavefronts (i.e., smaller angle, lower spatial frequency). Conversely, in the up-shifted case, a QWP at -45° increases $\theta_{\pm 1}$ (i.e., larger angle, higher spatial frequency).

Fourier transformation of the three interferograms produces the magnitude spectra presented in Fig. 6. The heterodyne frequency, as measured at the FPA, is $f_h = 9.9 \text{ mm}^{-1}$. Therefore, the prism's baseband spectrum is downshifted from $\pm 7.3 \text{ mm}^{-1}$ in (a) to $\mp 2.6 \text{ mm}^{-1}$ in (b), while in (c), the spectrum is upshifted to $\pm 17.2 \text{ mm}^{-1}$.

Spurious signatures (around 15% of peak) appear at $\pm 12.4 \text{ mm}^{-1}$ and $\pm 22.3 \text{ mm}^{-1}$ in the upshifted (c) case. These erroneous signals remain in the downshifted (b) case, and can be calculated by subtracting $2f_h$ from the aforementioned values. This yields false signatures at $\mp 7.4 \text{ mm}^{-1}$ and $\pm 2.5 \text{ mm}^{-1}$, respectively. Note that there is crosstalk between the false signatures at $\pm 2.5 \text{ mm}^{-1}$ and the heterodyned baseband spectrum at $\mp 2.6 \text{ mm}^{-1}$. These spurious signatures arise from imperfections in the PG, which allows some leakage into the $m = \pm 2$ diffraction orders. We expect that this can be reduced dramatically by optimizing the PG's fabrication techniques.

Future work is aimed at converting the presented SHI into a calibrated spatial heterodyne spectrometer [8,11]. A calibrated spectral reconstruction can be extracted

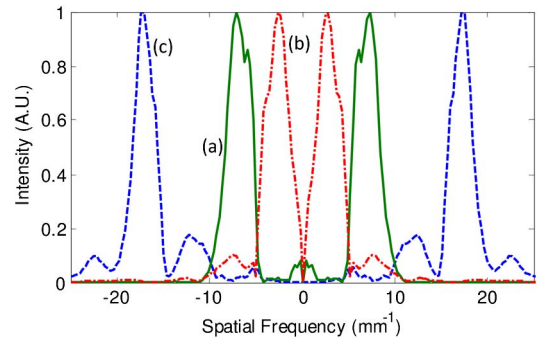


Fig. 6. (Color online) Spectrum of the interferograms in Fig. 5 versus the FPA's spatial frequency in mm^{-1} . (a) Prism only and no PG. (b) Prism and PG with QWP at 45° . (c) Prism and PG with QWP at -45° .

from the data represented in Fig. 6. Calibration will require unmixing the spurious signatures from the baseband spectrum. Advantages of the described SHI include its potential for extreme compactness, low thermal mass, minimal complexity, and, due to its common-path design, vibration and alignment insensitivity when compared to an FPE or a Michelson-based SHI. These advantages will yield improved space, air, microscope and telescope-based sensors for subangstrom spectrometry in atmospheric and astrometric studies, biomedical imaging, and remote sensing.

References

1. J. W. Meriwether, *J. Atmos. Sol. Terr. Phys.* **68**, 1576 (2006).
2. B. S. Gray, S. P. Spoor, and I. D. Latimer, *Meas. Sci. Technol.* **1**, 1072 (1990).
3. W. Liller, *Appl. Opt.* **9**, 2332 (1970).
4. P. Mouroulis, R. G. Sellar, D. W. Wilson, J. J. Shea, and R. O. Green, *Opt. Eng.* **46**, 063001 (2007).
5. M. W. Kudenov, J. Craven-Jones, R. Aumiller, C. Vandervlugt, and E. L. Dereniak, *Opt. Eng.* **51**, 044002 (2012).
6. G. Hernandez and R. G. Roble, *Appl. Opt.* **18**, 3376 (1979).
7. J. Beckers, L. Dickson, and R. Joyce, *Appl. Opt.* **14**, 2061 (1975).
8. C. R. Englert, D. D. Babcock, and J. M. Harlander, *Appl. Opt.* **46**, 7297 (2007).
9. P. B. Hays and R. G. Roble, *Appl. Opt.* **10**, 193 (1971).
10. J. M. Harlander, R. J. Reynolds, and F. L. Roesler, *J. Astrophys.* **396**, 730 (1992).
11. S. Watchorn, J. Noto, J. Anderson, and C. E. Sioris, *Proc. SPIE* **7812**, 781207 (2010).
12. C. Oh and M. J. Escuti, *Opt. Lett.* **33**, 2287 (2008).
13. M. W. Kudenov, M. J. Escuti, E. L. Dereniak, and K. Oka, *Appl. Opt.* **50**, 2283 (2011).
14. M. Kudenov, M. Escuti, N. Hagen, E. Dereniak, and K. Oka, *Opt. Lett.* **37**, 1367 (2012).
15. M. J. Padgett, A. R. Harvey, A. J. Duncan, and W. Sibbett, *Appl. Opt.* **33**, 6035 (1994).
16. P. R. Griffiths and J. A. de Haseth, *Fourier Transform Infrared Spectrometry* (Wiley-Interscience, 1986).
17. M. W. Kudenov and E. L. Dereniak, *Opt. Exp.* **20**, 17973 (2012).
18. H. Ono, T. Wada, and N. Kawatsuki, *Jpn. J. Appl. Phys.* **51**, 030202 (2012).